AGU PUBLICATIONS

JGR

Journal of Geophysical Research: Atmospheres

RESEARCH ARTICLE

10.1002/2015JD024397

Key Points:
- Climate variability induces significant uncertainty in multidecadal trends of atmospheric constituents
- Future trends in surface ozone are mainly driven by internal variability and emissions changes
- Attributing observed ozone trends to emissions changes requires consideration of climate variability

Correspondence to:
E. A. Barnes,
eabarnes@atmos.colostate.edu

Citation:
Barnes, E. A., A. M. Fiore, and L. W. Horowitz (2016), Detection of trends in surface ozone in the presence of climate variability, *J. Geophys. Res. Atmos.*, *121*, 6112–6129, doi:10.1002/2015JD024397.

Received 26 OCT 2015
Accepted 21 MAR 2016
Accepted article online 28 MAR 2016
Published online 26 MAY 2016

Detection of trends in surface ozone in the presence of climate variability

Elizabeth A. Barnes[1], Arlene M. Fiore[2], and Larry W. Horowitz[3]

[1]Department of Atmospheric Science, Colorado State University, Fort Collins, Colorado, USA, [2]Department of Earth and Environmental Sciences and Lamont-Doherty Earth Observatory of Columbia University, New York, New York, USA, [3]NOAA Geophysical Fluid Dynamics Laboratory, Princeton, New Jersey, USA

Abstract Trends in trace atmospheric constituents can be driven not also by trends in their (precursor) emissions but also by trends in meteorology. Here we use ground-level ozone as an example to highlight the extent to which unforced, low-frequency climate variability can drive multidecadal trends. Using output from six experiments of the Geophysical Fluid Dynamics Laboratory chemistry-climate model (CM3), we demonstrate that 20 year trends in surface ozone driven by climate variability alone can be as large as those forced by changes in ozone precursor emissions or by anthropogenic climate change. We highlight regions and seasons where surface ozone is strongly influenced by climate variability and thus where a given forced trend may be more difficult to detect. A corollary is that this approach identifies regions and seasons of low variability, where measurement sites may be most effectively deployed to detect a particular trend driven by changing precursor emissions. We find that the representative concentration pathways 4.5 (RCP4.5) and RCP8.5 forced surface ozone trends in most locations emerge over background variability during the first half of the 21st century. Ozone trends are found to respond mostly to changes in emissions of ozone precursors and unforced climate variability, with a comparatively small impact from anthropogenic climate change. Thus, attempts to attribute observed trends to regional emissions changes require consideration of internal climate variability, particularly for short record lengths and small forced trends.

1. Introduction and Motivation

Observed trends in reactive trace atmospheric constituents reflect a combination of two underlying drivers: (1) trends in precursor emissions and (2) trends in meteorology. Ideally, the chemistry-climate models that are now being used to project future atmospheric composition and climate [e.g., *Lamarque et al.*, 2013] would reproduce observed trends in atmospheric constituents, lending confidence to future projections. *Parrish et al.* [2014], however, find that three state-of-the-art chemistry-climate models (CCMs) systematically underestimate the observed lower tropospheric ozone trends over the past few decades. *Wild et al.* [2012] found that multiple chemistry-transport models (CTMs), when driven with estimated anthropogenic emission changes from 1960 to 2000, were able to reproduce lower tropospheric ozone trends broadly consistent with observations at a remote site (Mauna Loa) but underestimated the observed trend at a midlatitude site (Mace Head). Since CTMs are typically driven with a single year's meteorology that repeats each year while emissions are allowed to change, *Wild et al.* [2012] noted that discrepancies between observed and CTM-based trends could indicate a role for meteorological variability [see also *Lin et al.*, 2014] and natural emissions in driving differing regional trends.

Discrepancies between modeled and observed ozone trends may thus indicate a combination of factors: (1) measurement uncertainties and sampling biases, for example, the representativeness of ozone trends derived from sparse measurements [e.g., *Lin*, 2015b]; (2) errors in the trends incorporated in the underlying emission inventories used in the model; (3) poor model representation of the processes (chemical, physical, and dynamical) that control the observed trend at a given location; and (4) trends driven by low-frequency climate variability. For example, measurement sites may be influenced by decadal-scale climate variability, driven by tropospheric circulation changes, as found during spring and fall at Mauna Loa [*Lin et al.*, 2014], or changes in the stratospheric contribution to surface ozone [*Hess et al.*, 2015; *Lin et al.*, 2015a]. While factors (1), (2), and (3) may be improved with better inventories and process representation in models, factor (4) encompasses variability that a chemistry-climate model (i.e., a model generating its own weather) is not

expected to reproduce exactly. The influence of meteorology on ozone trends can occur not only through transport but also through modifications to the meteorological conditions to which near-surface ozone chemistry is most sensitive (e.g., sunlight, temperature, boundary layer mixing, and humidity). Meteorological variations can also induce changes in emissions of ozone precursors, while the radiative effects of ozone, a strong greenhouse gas in the upper troposphere, may also feed-back, further modifying the meteorology. Long-term trends in the meteorology can be driven by external forcings, such as anthropogenic climate change, or internal climate variability such as the Pacific Decadal Oscillation.

Presently, the International Global Atmospheric Chemisty/Stratospheric Processes and their Role in Climate Chemistry-Climate Model Initiative (CCMI) is coordinating the evaluation and intercomparison of chemistry-climate models. Many of the models providing simulations for CCMI [*Eyring et al.*, 2013] are fully coupled chemistry-climate models and thus will exhibit variability distinct from the observations as well as from the other models and across ensemble members. Thus, the goal of this work is to provide a framework for comparing coupled models to one another and to the observations in the presence of climate variability. Specifically, our interest here is how internal (unforced) climate variability can influence our ability to detect surface ozone trends forced either by changes in ozone precursor emissions or by forced changes in the climate (i.e., due to anthropogenic greenhouse gases and aerosols). Using the Geophysical Fluid Dynamics Laboratory (GFDL) chemistry climate model, one of those previously evaluated by *Parrish et al.* [2014]), we demonstrate that 20 year trends in surface ozone arising from climate variability can be as large as those forced by changes in ozone precursor emissions or by anthropogenic climate change over the same time period. We highlight regions and seasons where surface ozone is most sensitive to this "climate noise" and thus where forced trends may be more difficult to detect than in other regions. Conversely, regions with less climate variability may be ideal for monitoring long-term changes in reactive trace atmospheric constituents since they should require a shorter data record for the same forced signal to emerge from the climate noise. We finish by quantifying the length of time needed for future forced surface ozone trends to emerge from background climate variability under three emissions scenarios.

2. Data and Methods

2.1. Model and Simulations

We analyze simulated daily mean surface ozone from a suite of simulations from 1950 to 2055 performed using the Geophysical Fluid Dynamics Laboratory (GFDL) Climate Model version 3 (CM3) chemistry-climate model [*Donner et al.*, 2011], which includes fully coupled tropospheric and stratospheric chemistry [*Austin et al.*, 2013; *Naik et al.*, 2013]. Specifically, we analyze model output from six different experiments as summarized in Table 1. The Historical simulations (five ensemble members) are the same as those analyzed by *John et al.* [2012], *Levy et al.* [2013], and *Turner et al.* [2013] while the future simulations (representative concentration pathways 4.5 (RCP4.5), RCP4.5_WMGG (well-mixed greenhouse gas) , RCP8.5, and RCP8.5_WMGG; three ensemble members each) are the same as in [*Clifton et al.*, 2014]. In the WMGG (well-mixed greenhouse gas) simulations, only the well-mixed greenhouse gases and land use evolve along their respective RCP pathways, while aerosol and ozone precursor emissions are held fixed at 2005 levels in the WMGG simulations. Methane concentrations seen by the radiation follow the RCP scenario, while those used for chemistry remain fixed at 2005 levels. We include here an additional control simulation (Control-1990) in which all emissions and abundances of greenhouse gases and ozone depleting substances are set to 1990 values and the model is run for 500 years (of which we use 200). The Control-1990 simulation enables us to evaluate ozone trends driven solely by internal (unforced) meteorological variability. In all simulations, biogenic (e.g., isoprene, and soil NO_x) emissions and dry deposition velocities vary monthly (and diurnally for isoprene emissions and ozone dry deposition) but not from year-to-year. Biomass burning emissions are prescribed to decadally varying climatological values. Prescribing these emissions necessarily underestimates year-to-year variability and so points to our estimates of climate variability of surface ozone being conservative. Finally, lightning NO_x and emissions of dust, sea salt, and dimethylsulfide are tied to the model meteorology.

2.2. Calculation of Trends

All trends are defined as the slope of the linear least squares regression of seasonal means. For some of the analysis, we compute all possible 20 year trends over a time series, where each year acts as the start year for a trend calculation. For example, we obtain 81 different 20 year trends for each season from a 100 year time series. This calculation is performed separately for each ensemble of each scenario available (refer to Table 1). Twenty year trends were chosen, as this period represents a multi-decadal time scale over which we

Table 1. Description of the GFDL CM3 Simulations Analyzed Here

Experiment	Number of Members	Years	Description
Control-1990	1	200 years	All emissions set to 1990 values
Historical	5	1950–2004	Historical emissions
RCP4.5	3	2006–2055	RCP4.5 emissions
RCP4.5_WMGG	3	2006–2055	RCP4.5 with ozone and aerosol precursors fixed at 2005 levels
RCP8.5	3	2006–2055	RCP8.5 emissions
RCP8.5_WMGG	3	2006–2055	RCP8.5 with ozone and aerosol precursors fixed at 2005 levels

have quality observations of surface ozone throughout the Northern Hemisphere [e.g., *Parrish et al.*, 2012]. However, the choice of 20 year trends (as compared to, for example, 10 or 30 year trends) does not change the overall conclusions of this work.

The statistical significance of the forced trends in the RCP scenarios compared to what would be expected due to Gaussian internal variability is assessed with the standard error of the regression using a two-tailed 95% confidence level. We note that it does not make sense to calculate the statistical significance of the trends in the Control-1990 simulation, as these trends are the Gaussian internal variability itself.

2.3. Quantification of the Time of Emergence

At its most basic level, the time of emergence is a function of two fundamental quantities: (1) the internal variability of surface ozone and (2) the magnitude of the forced response. If the internal variability is large, or the forced response is small, it will take longer for the forced signal to emerge from the background noise. Alternatively, if the internal variability is small, or the forced response is large, it will take less time for the forced signal to emerge.

Various definitions for the time of emergence exist. For this work, we define the time of emergence of a forced trend following *Thompson et al.* [2015]. Specifically, they demonstrated that if a time series is composed of a constant linear trend (b) with Gaussian variability about the trend, the spread in the realized trends can be calculated analytically. This spread is a function of the standard deviation of the internal (unforced) variability and the lag-1 autocorrelation of the variability about the trend. Thus, one possible definition for the time of emergence (TOE) of the forced trend is the amount of time it takes for the 95% confidence interval for the trend to no longer pass through zero. We note here that a forced trend in ozone might arise either from ozone precursor emission changes or from anthropogenic climate change.

We estimate the future forced trend in surface ozone as the linear slope of the ensemble mean trend over 2006–2055 separately in RCP4.5 and in RCP8.5. Averaging over the ensemble members removes some of the internal variability, providing a better estimate of the forced trend than any one member. The internal variability of seasonal mean surface ozone (σ) and the lag-1 autocorrelation (r_1) are estimated from the statistics of the Control-1990 simulation. Finally, we convert the time of emergence to a "year of emergence" defined as the year the trend will emerge from the background noise assuming a start year of 2006.

This estimate of the time of emergence holds under the following three assumptions: (1) forced trends are roughly linear, (2) the internal variability is well approximated as a Gaussian process, and (3) the standard deviation and autocorrelation are stationary in time. Below, we briefly outline why these three assumptions hold in the case of seasonal mean surface ozone over the period analyzed.

To ensure that surface ozone trends across the globe are linear over the 2006–2055 period (assumption #1), we fit both linear and second-order polynomials to the surface ozone time series at each grid box and find that the second-order polynomials offer little additional variance explained compared to the linear fits (not shown). While this assessment does not preclude the possibility of higher-order trends, we conclude that the assumption of a linear trend over this 50 year period is appropriate. We note that simulated surface ozone trends out to 2100 are not linear at many locations (e.g., Lassen, California), and thus, we restrict our analysis to the 2006–2055 period over which trends at many locations are well captured by a linear trend.

To test that the variability of seasonal mean surface ozone is well described by Gaussian noise (assumption #2), we applied a Kolmogorov-Smirnov test against a standard normal distribution (not shown). Modeled surface ozone exhibits Gaussian variability with near-zero lag-1 year autocorrelations (absolute value less than 0.2) over most the globe (greater than 95% of the model grid cells). We note that even with zero autocorrelation,

large multidecadal trends can still emerge in a random time series. In the rare instances where the surface ozone variability significantly differed from the standard normal or the lag-1 autocorrelation was less than −0.2 (signifying potential oscillatory behavior), the grid boxes were masked out of the relevant figures.

Finally, it is a potential concern that changes in mean surface ozone concentrations could influence the magnitude of surface ozone variability in the future or that climate change could significantly modify the dynamics that lead to this variability. If this were the case, our assumption of a constant standard deviation (assumption #3) would not hold. In an effort to check that the variability of surface ozone remains relatively constant in the future simulations given the expected changes in mean surface ozone, we additionally estimated σ from the detrended surface ozone in RCP4.5_WMGG and RCP4.5. We then calculated the time of emergence using these estimates of σ and find similar results (not shown) to those calculated using σ from the Control-1990 simulation. We conclude that our estimate of the internal variability of surface ozone is adequate to estimate present-day and future surface ozone variability in these simulations.

2.4. Significance of Correlations of Trends

We analyze the circulation patterns associated with multidecadal trends in surface ozone by computing the correlation between the 20 year trend time series of surface ozone and the 20 year trend time series of 500 hPa zonal wind or geopotential height. In this case, one cannot use the standard approach for assessing the significance of the Pearson correlation since the time series of 20 year trends are highly autocorrelated (each trend shares 19 of its 20 data points with the adjacent trend). Hence, we take a Monte Carlo approach in determining the significance of the correlation and create two synthetic time series that exhibit Gaussian noise with a lag-1 autocorrelation of 0.4 (to be very conservative in our significance test). We then calculate the correlation of the 20 year trends of these two synthetic time series and repeat this process 5000 times. The 95% confidence interval on the correlation determined from this Monte Carlo approach is approximately ±0.4, which is the cutoff used to determine significance in Figure 7.

3. Model Evaluation

We first discuss the ability of the GFDL CM3 model to simulate seasonal mean surface ozone variability. Figure 1 displays time series of surface ozone at seven remote Northern Hemisphere sites. Five of the seven were analyzed and discussed in detail by *Parrish et al.* [2012] (see Table 2), except that the time series at Lassen National Park in California has been extended to 2014 using data obtained from the National Parks Service for Lassen Volcanic National Park – Manzanita Lake Fire Station, and the time series at Jungfraujoch, Switzerland, has been extended to 2014 using data obtained from the World Data Centre for Greenhouse Gases (http://ds.data.jma.go.jp/gmd/wdcgg/). While the 21st century trends are roughly linear (see discussion in section 2), the trends over the historical period are not, and thus, we detrend the time series by removing the best fit second-order polynomial in order to focus on the year-to-year variability. The solid curves in Figure 1 denote the observations, and the thin lines display three independent ensembles of the GFDL CM3 model. The three independent ensemble members were created by combining the Historical and RCP4.5 ensembles together, as the observational record spans these two forcing scenarios. The model is sampled at the grid cell nearest each monitoring site and at the model level closest to its altitude above sea level. In addition, the observations and model are sampled identically in time, such that missing years are removed in each.

The model appears to capture the interannual variability of surface ozone in winter (black) at all seven sites, although in summer (red) it may underestimate the variability (e.g., Zugsptize). We further quantify this comparison in Figure 2, where we show the standard deviation of detrended seasonal mean surface ozone from the observations (circles) and the model (squares). Filled markers denote where the modeled and observed variability are not statistically different from one another at 95% confidence using an *F* test. While there are multiple seasons and locations where the model captures the observed variability, there are other locations where it does not. In nearly every instance where the model and observations disagree, the model underestimates the variability. This underestimation may be due, in part, to the fact that the model is sampled over a grid box and is in this way an average of many points, while the observations are single point measurements. We have confirmed that the standard deviation decreases as one averages over larger and larger areas and thus that the model would on average exhibit lower variability than that observed.

Previous studies have also documented the ability of GFDL CM3 (or AM3—the atmospheric component of CM3) to simulate surface ozone variability. *Barnes and Fiore* [2013] demonstrated that the relative standard deviation (the standard deviation normalized by the mean) of June–August (JJA) surface ozone over the

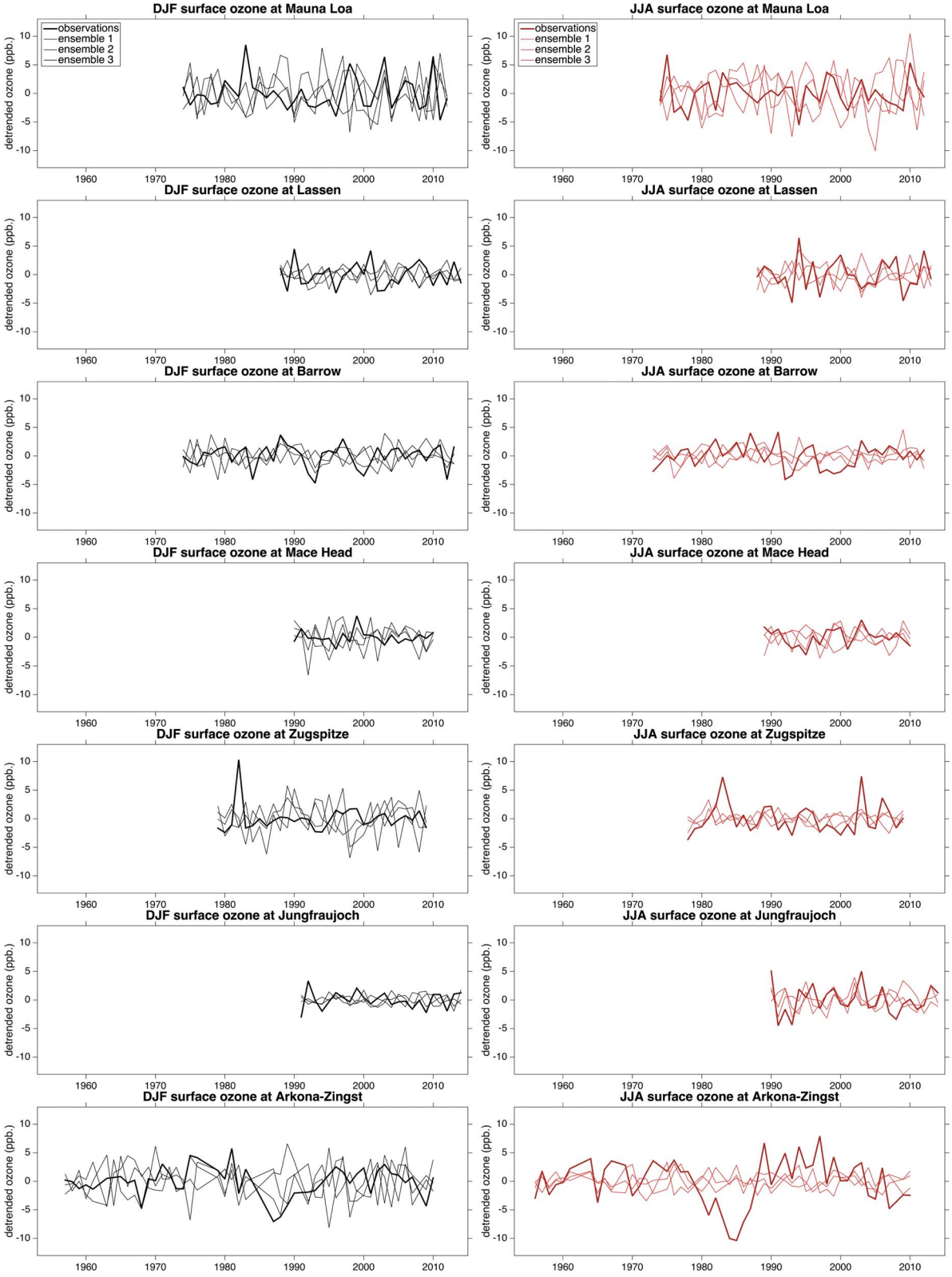

Figure 1. Time series of detrended seasonal mean surface ozone at seven sites across the Northern Hemisphere from observations (thick line) and from three independent ensemble members of the GFDL CM3 model (thin lines). The model has been sampled at the altitude and latitude/longitude closest to that of the observations and over the same years.

Table 2. Observational Surface Ozone Data Sets [See *Parrish et al.*, 2012 for Details][a]

Monitoring Site	Record Length	Latitude/Longitude	Elevation (km)
Mauna Loa, Hawaii	1974–2012	21°N, 158°W	3.34 km
Lassen, California	1988–2014	40°N, 121°W	1.76 km
Barrow, Alaska	1974–2013	71°N, 157°W	0.00 km
Mace Head, Ireland	1990–2010	53°N, 9°W	0.02 km
Zugspitze, Germany	1979–2009	47°N, 10°E	3.0 km
Jungfraujoch, Switzerland	1990–2014	46°N, 7°E	3.6 km
Arkona-Zingst, Germany	1957–2010	54°N, 12°E	0.00 km

[a]The Mauna Loa and Barrow data sets were provided by *McClure-Begley et al.* [2014].

Eastern United States was well captured by CM3 when compared with the United States Environmental Protection Agency Clean Air Status and Trends Network data set. *Lin* [2015b], *Fiore et al.* [2014] and *Lin et al.* [2012] showed similar spring time variability in ozone mixing ratios over the Western United States in AM3 compared to those observed. *Naik et al.* [2013] further compared the interannual variability of surface ozone in AM3 to that observed across multiple Northern Hemisphere regions (e.g., Northern Europe, Mountainous Europe, and India). While they found that AM3 has a tendency to overestimate midlatitude concentrations, a common feature among chemistry-climate models [e.g., *Lamarque et al.*, 2012], inspection of their Figure 4 suggests that the model represents much of the year-to-year variability, with underestimates at a few locations (e.g., the Mediterranean region).

Here we are interested in the impacts of decadal climate variability on surface ozone trends, and thus, we conclude from our evaluation that although CM3 tends to underestimate surface ozone variability at some Northern Hemisphere sites in some seasons, it is adequate to lay the groundwork for quantifying decadal trends in surface ozone driven by climate variability. Furthermore, the potential underestimation of internal variability by the model suggests that in the real world, internal climate variability, if anything, plays an even more important role.

4. Results

4.1. Changes in Ozone Over Time

We focus our initial analysis on Lassen, California, a remote site in the lower free troposphere at which ozone has been measured since the late 1980s. Figure 3 shows the time evolution of modeled ozone at Lassen as a function of season. Simulated lower free-tropospheric ozone has been steadily increasing at Lassen since

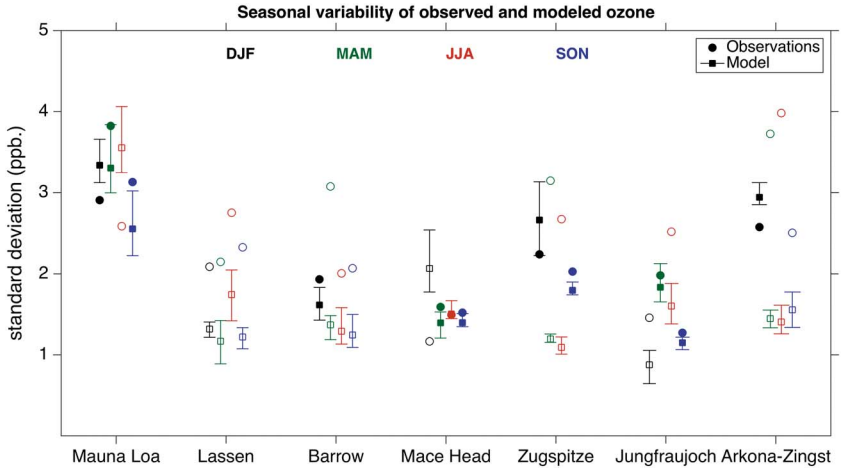

Figure 2. The standard deviation of the detrended seasonal mean surface ozone from observations (circles) and three independent ensemble members from the model (squares; see text for details). The bars denote the range of ° standard deviations across the three members. Colors specify the season: winter (black), spring (green), summer (red), and fall (blue). Filled markers denote where the modeled and the observed standard deviations are not statistically different from each other at 95% confidence.

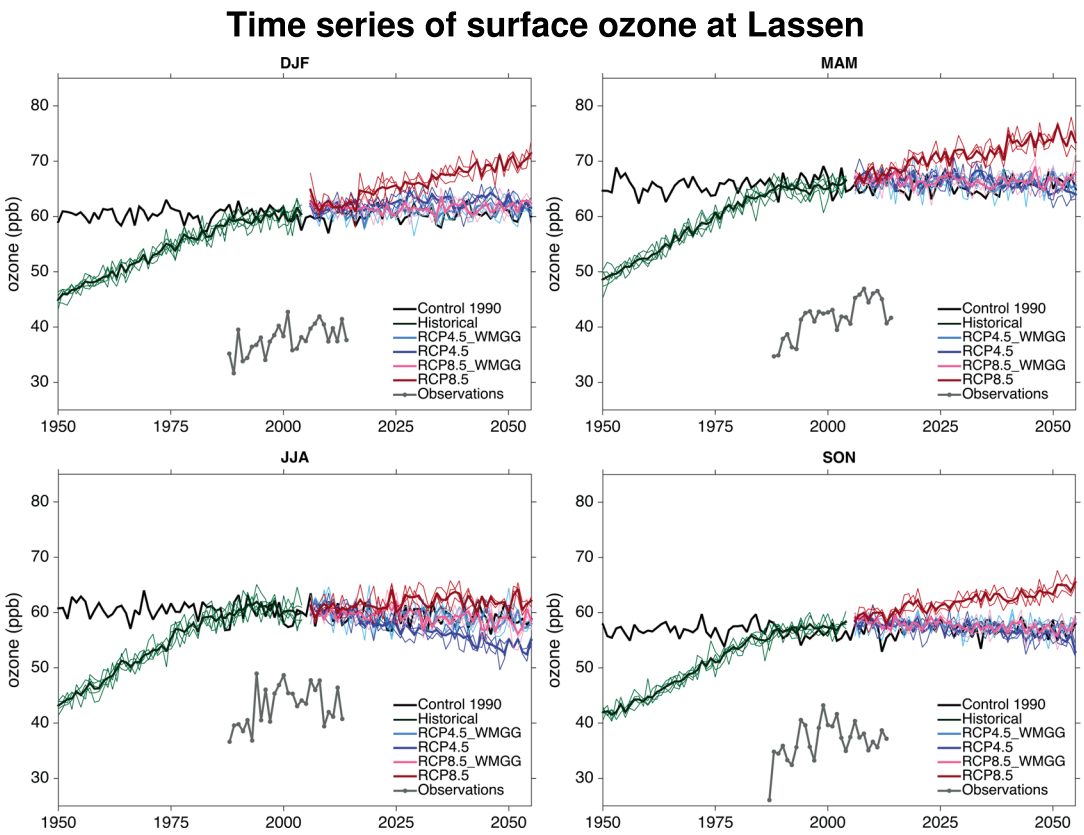

Figure 3. Time series of seasonal-mean surface ozone concentrations at Lassen (40°N, 121°W, 1756 m above sea level) from the GFDL CM3 model. Years for the 200 year Control-1990 simulation are arbitrary and only the first 105 years are shown. Thin lines denote individual ensembles while the thick lines denote the ensemble mean. Also shown in gray are the observations.

1950, as depicted by the Historical simulations (green). The gray curve denotes observed surface ozone. The model exhibits a similar trend as the observations (to be discussed), despite a positive bias in surface ozone over the northwestern United States [*Naik et al.*, 2013].

The future evolution of ozone at Lassen depends on projected changes of ozone precursor emissions. In RCP4.5 (dark blue), ozone at Lassen modestly declines in all seasons except winter (December–February, DJF). Under the RCP4.5 scenario, global anthropogenic NO_x emissions (where we exclude shipping emissions) decrease by 41% and global methane abundance increases by 4% from 2005 to 2055. Asian emissions of anthropogenic NO_x, which are thought to play a dominant role in driving ozone trends at Lassen [e.g., *Cooper et al.*, 2010; *Parrish et al.*, 2012], also decrease by 66% although they only begin to decrease in the 2020s. North American anthropogenic emissions of NO_x decrease by 71% between 2005 and 2055.

Under RCP8.5 (red), surface ozone increases at Lassen in all seasons despite global anthropogenic NO_x emissions decreasing by 28%. This increase is driven by global methane abundance increasing by 66% from 2005 to 2055. Asian emissions of anthropogenic NO_x decrease by 44%, and North American emissions decrease by 56%. While these simulations cannot distinguish the importance of local versus nonlocal emissions in driving surface ozone trends, they suggest that the methane increases under RCP8.5 dominate over the NO_x decreases to drive increasing surface ozone at Lassen.

When ozone precursor emissions are held fixed in RCP4.5_WMGG (light blue) and RCP8.5_WMGG (pink), surface ozone shows smaller changes between 2006 and 2055 than in the full RCP4.5 and RCP8.5 scenarios. Any trends in RCP4.5_WMGG or RCP8.5_WMGG are due solely to changes in the meteorology. Trends in meteorology arise from changes in forcings (e.g., by increasing greenhouse gases), in addition to internal climate variability (climate noise). Finally, surface ozone in the Control-1990 simulation (black) exhibits no long-term trends throughout the 200 years analyzed, reflecting the perpetually repeating 1990 level of ozone precursor emissions and greenhouse gas abundances.

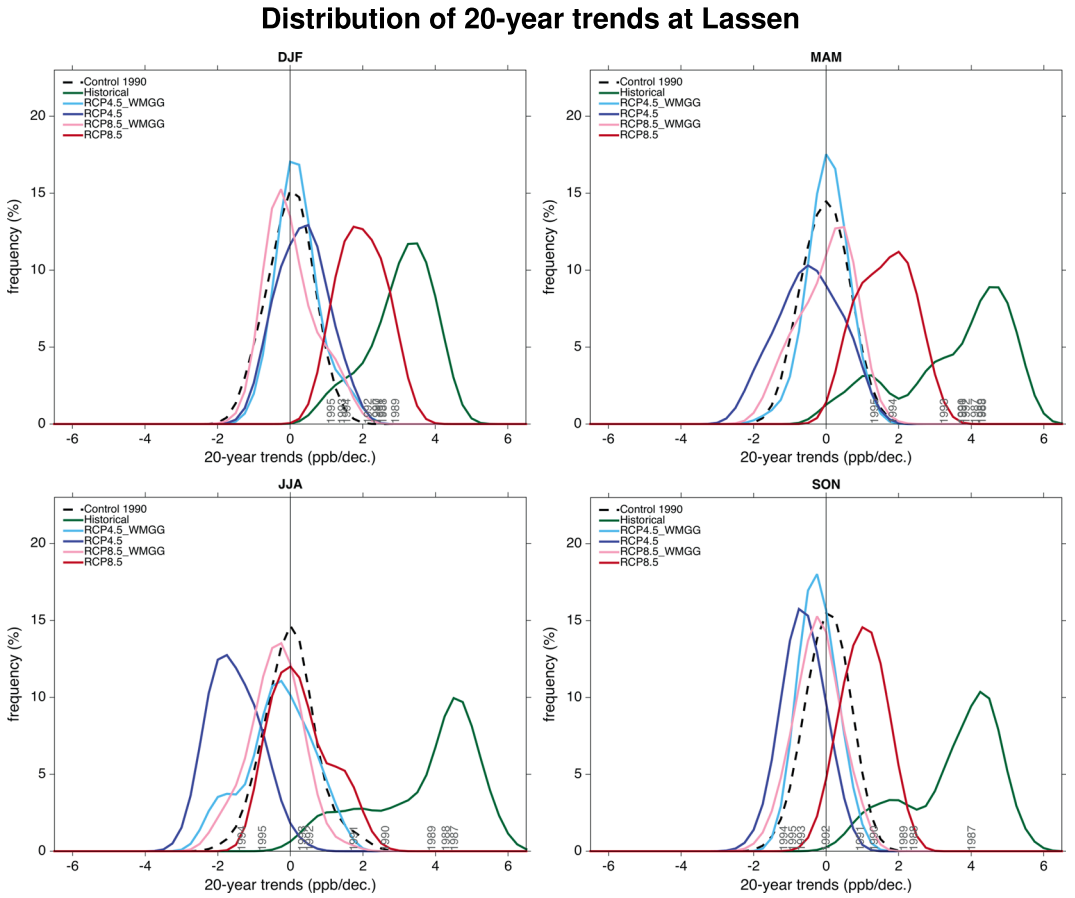

Figure 4. Frequency of 20 year trends in surface ozone from the GFDL CM3 simulations, sampled at the grid box closest to the location and altitude of Lassen, CA, and binned every 0.25 ppb/decade. Histograms have been smoothed with a 1-2-1 filter applied forward and backward four times. Observed trends are denoted by the starting year of the 20 year period (gray text).

4.2. Spread in 20 Year Trends

Figure 4 shows the distribution of all possible 20 year trends at Lassen across all the years of the different simulations (as described in section 2.2). We begin by focusing on the mean 20 year trend, which can be approximated by the peak in the histograms in Figure 4 and is plotted in Figure 5a. The mean trend is an estimate of the 20 year forced response of surface ozone to changes in precursor emissions and/or climate. In all seasons, the Control-1990 simulation (black dashed) exhibits a mean 20 year trend of zero, reflecting the lack of forced trend as ozone precursor emissions and greenhouse gases are held fixed at 1990 values. Nevertheless, a wide range of possible trends result solely from climate variability in the CM3 model. This variability represents the climate noise in the chaotic climate system, as discussed further below.

In the Historical simulations (green; Figure 3), the average 20 year trend is positive in all seasons. This increase in surface ozone is largely due to changes in emissions over the 1950–2004 period. Also shown as gray text in Figure 4 are the observed 20 year trends in surface ozone at Lassen, California. Each year denotes the start year of a 20 year trend in the observations over the period 1988–2014. The majority of the observed trends at Lassen fall within the simulated Historical trend distribution (green), indicating that the model can capture the sign and magnitude of the observed trends. Note, however, that the observed trends tend to fall in the left half of the modeled trend distribution. This is not necessarily an indication of model bias but rather likely reflects that the observed trends are calculated over a period (1988–2014) when the forced trends were smaller (see Figure 3). Thus, unlike the RCP scenarios which exhibit linear trends over the 2006–2055 period, the trends in the Historical simulation are not linear, increasing linearly from 1950 but leveling off in the 1990s.

In the future climate simulations, Figure 4 shows that for RCP4.5 (dark blue), the average 20 year trend (over the 2006–2055 period) is negative in all seasons but winter, reflecting the long-term decrease in surface

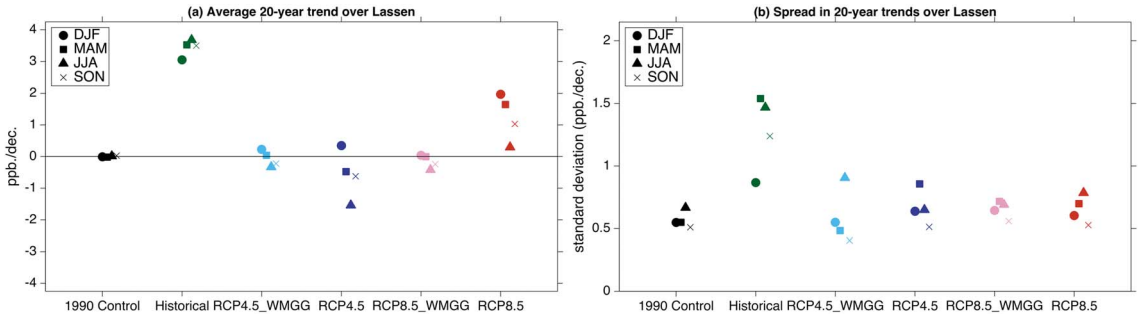

Figure 5. (a) Average and (b) standard deviation of 20 year surface ozone trends over Lassen, CA, as a function of season and model simulation.

ozone at Lassen likely driven by NO_x emission reductions. On the other hand, for RCP8.5 (red), the average 20 year trend is positive in all seasons, reflecting the long-term increase in tropospheric ozone driven by projected increasing methane abundances as previously discussed. The average 20 year trend in RCP4.5_WMGG (light blue) and RCP8.5_WMGG (pink) is near zero, similar to the Control-1990 simulation, as all of these experiments hold ozone and aerosol precursor emissions fixed. Note, however, that the climate is responding to increasing greenhouse gas concentrations in RCP4.5_WMGG and RCP8.5_WMGG, and thus, the near-zero average trend implies that 20 year surface ozone changes driven by the forced meteorological response to climate change are negligible over Lassen.

While the average 20 year trends reflect the trends in emissions (or lack thereof), surface ozone exhibits a wide range (spread) of 20 year trends in each of the six simulations. For example, although the forced trends in surface ozone over the twentieth century are positive, negative trends occur for individual 20 year periods in the Historical simulations (green; Figure 4). Note that the wider spread in this simulation versus the Control-1990 simulation reflects changes in emission trends over different 20 year periods; for example, larger emission trends occur in the earliest 20 year periods of the Historical simulation (i.e., the 1950s) when global emissions are ramping up, and smaller trends occur at the end of the twentieth century. In RCP4.5, a scenario with an emissions-driven ozone decrease, many positive 20 year trends still occur, some as large as 2 ppb/decade. Even in the controlled setting of the Control-1990 simulation where emissions and forcings are held constant, one can find both positive and negative 20 year trends as large as 2 ppb/decade. This spread in the Control-1990 simulation can be entirely attributed to internal climate variability. We quantify this spread by the standard deviation of the 20 year trends (width of the histograms in Figure 4) and plot the seasonal values in Figure 5b. The standard deviation of 20 year trends in the control is approximately 0.5 ppb/decade, signifying the large range of possible 20 year trends in Figure 4.

The standard deviations of the 20 year trends from the other five simulations are similarly plotted in Figure 5b. The similarity between the spread in the control and the spread in the other simulations strongly suggests that internal climate variability accounts for the majority of the spread in 20 year trends across the future climate simulations. Also evident from Figure 5b is that the spreads in RCP4.5 and 8.5 are similar to those in RCP4.5_WMGG and 8.5_WMGG, highlighting that future changes in ozone precursor emissions do not greatly affect the spread in 20 year trends at Lassen. Finally, we note that the standard deviations of 20 year trends over the Historical period (green) are more than double those of the Control-1990 for three out of the four seasons. This difference is not due to differences in internal climate variability but rather, as discussed above, to the fact that the forced ozone trends are not linear over the 1950–2004 period. Thus, the range of forced trends in different periods of the Historical simulations account for the additional spread in 20 year ozone trends.

Extending this analysis to the Northern Hemisphere, we estimate 20 year trends in surface ozone by sampling trends in each grid cell in the lowest model layer. Figure 6 shows the standard deviation of 20 year surface ozone trends for all continental grid cells calculated using the Control-1990 simulation. The largest spread in 20 year trends is found in winter (DJF) over western Europe and central Africa and in summer (JJA) over Russia. Large values indicate regions where meteorology can drive a wide range of 20 year trends in the absence of any changes in ozone precursor emissions, through changes in either transport or chemistry. Conversely, small values indicate regions where meteorological variability appears to play a minor role.

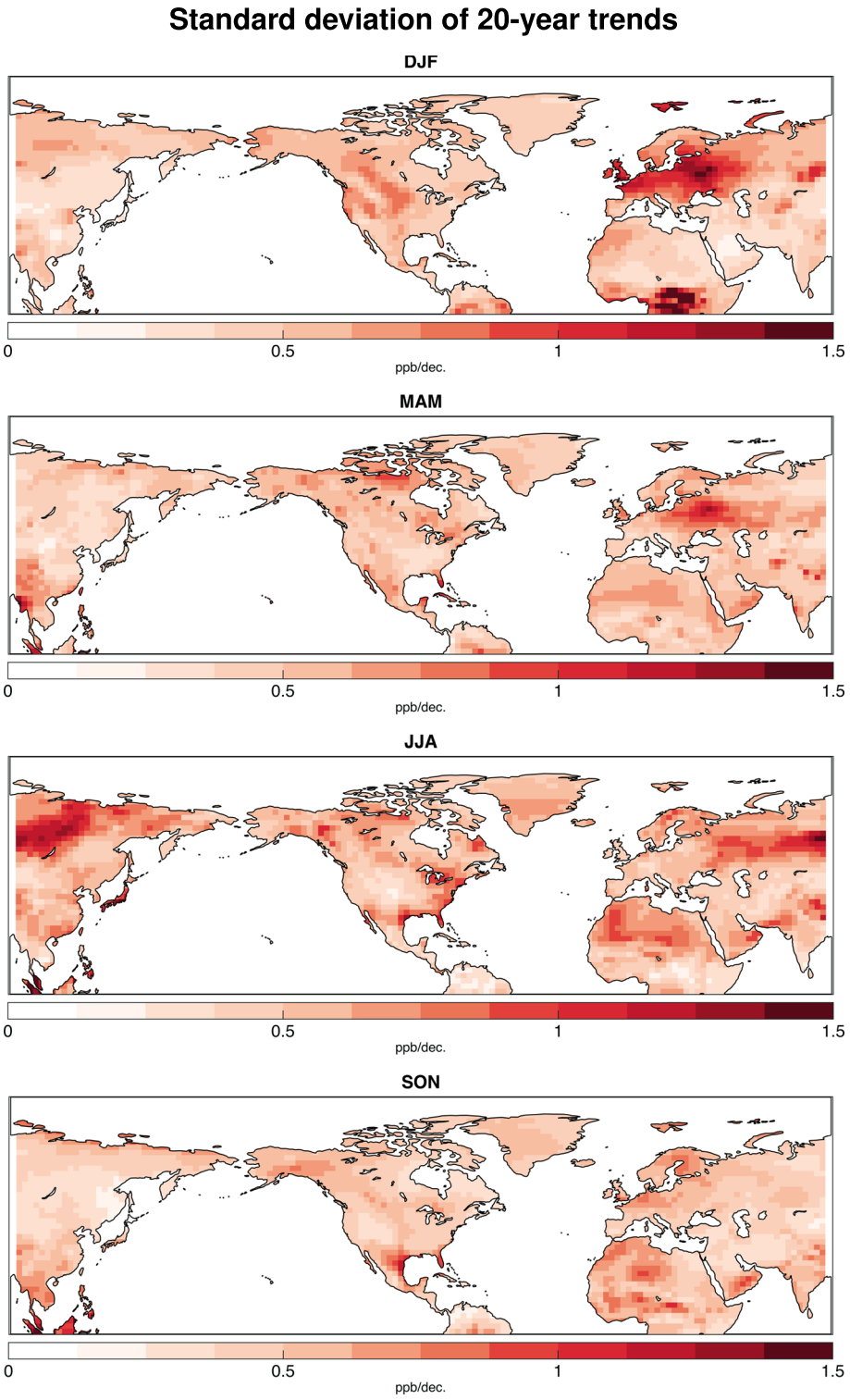

Figure 6. The standard deviation of 20 year trends in surface ozone from the Control-1990 simulation.

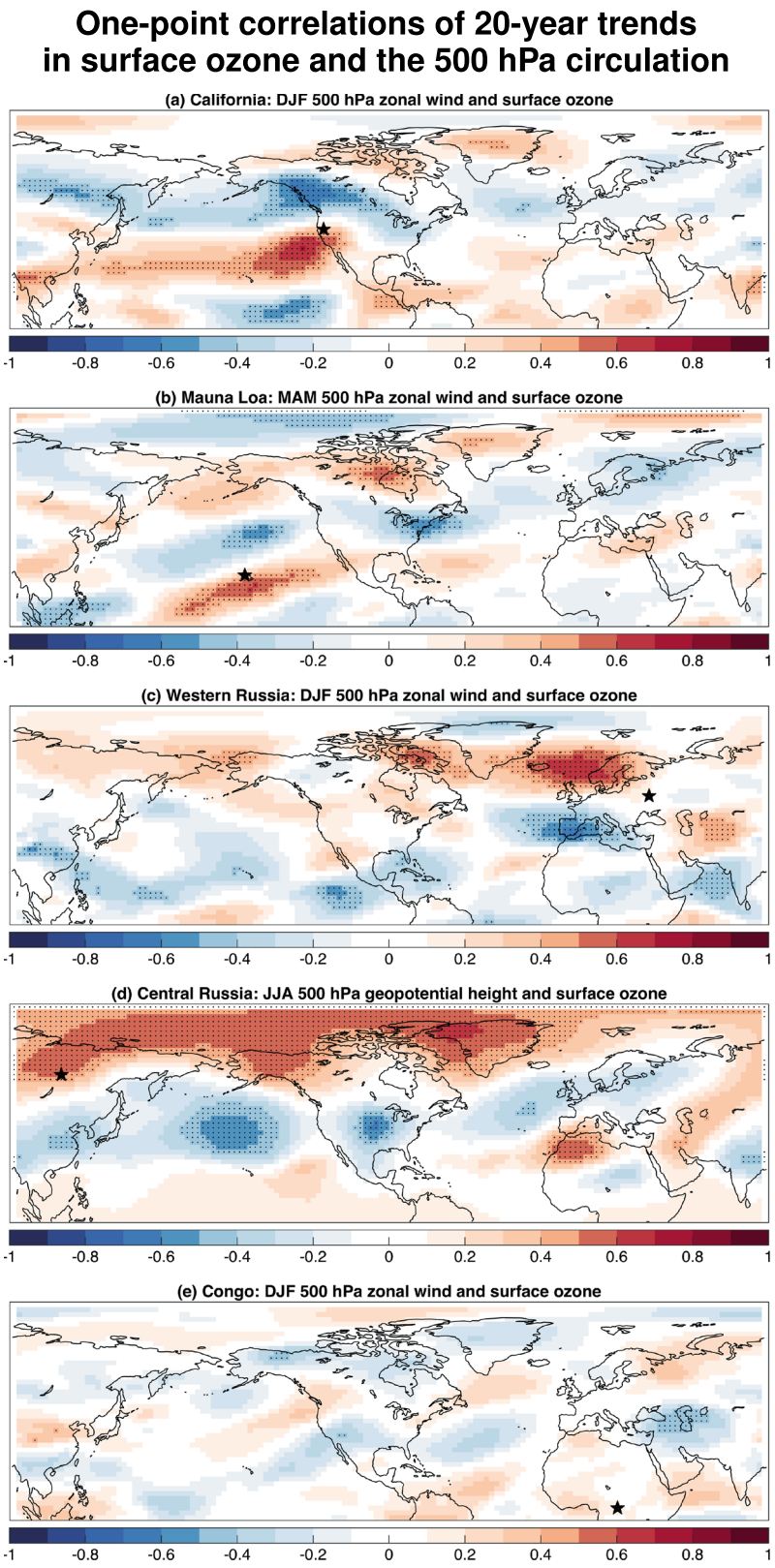

Figure 7. One-point correlation plots of 20 year trends in surface ozone at select grid points (black stars) and the 20 year trends in the circulation at all other grid points. Stippling denotes correlations that are significant at the 95% confidence level using a bootstrap approach to take into consideration the autocorrelation of the time series of trends (see section 2.4).

To quantify the meteorological conditions that are driving the range of 20 year trends in Figure 6, we compute the 20 year trends in the 500 hPa zonal wind and geopotential height fields at each grid point. Figure 7 presents one-point correlation maps of the 20 year surface ozone trends at five different sites (denoted by the black stars) correlated with 20 year trends in the circulation over the globe. Focusing first on California (Figure 7a), we see that large positive 20 year trends in winter time surface ozone there (black star) is highly correlated with positive 20 year trends in zonal wind (increased westerlies) to the south and negative 20 year trends to the north. This pattern implies an equatorward shift and extension of the jet stream over the North Pacific. Positive trends in surface ozone at Mauna Loa in spring (Figure 7b) are highly correlated with positive trends in zonal wind to the south and negative trends to the north. This pattern is associated with a narrowing of the subtropics (equatorward jet shift) and is dynamically consistent with the observational study of *Lin et al.* [2014], who showed that an expansion of the tropics in the 2000s resulted in negative decadal trends in surface ozone at Mauna Loa.

Moving to Europe and Asia, the large range of DJF trends over Western Russia (see Figure 6) appear to be linked with variability in the North Atlantic jet stream. The 500 hPa zonal winds show that a poleward shift of the jet stream results in large 20 year trends in surface ozone (Figure 7c). Over central Russia (Figure 7d), large trends in surface ozone are highly correlated with large negative trends in the Northern Annular Mode pattern seen most clearly as positive height anomalies over the pole and negative height anomalies in the midlatitudes.

Finally, we investigate the large variability in surface ozone in DJF over the Congo (refer to Figure 6). Unlike the four midlatitude sites, 20 year trends in surface ozone over the Congo are not significantly correlated with trends in zonal wind or geopotential height. This is not surprising, as one would expect local processes such as convection to play a more dominant role in driving surface ozone variability in the tropics and the large-scale circulation to be more important in the midlatitudes.

The results from this section have two major implications: (1) Attributing an observed multidecadal trend to particular changes in emissions is challenging given that climate variability can drive trends of similar magnitude, and (2) comparisons of trends across CCMs and with observations must account for the range of uncertainty due to climate variability.

4.3. Detection of Forced Surface Ozone Trends

We next quantify the time of emergence of forced surface ozone trends as a function of season and geographic location. The time of emergence is a quantity that has been used extensively in the recent climate literature and quantifies how long one must wait for a forced signal to "emerge" from the background climate variability. In this case, our interest is how long one must wait for forced trends in surface ozone to be confidently distinguished from those driven by internal climate noise.

To demonstrate the regions where internal variability is most important for potentially masking forced surface ozone trends, we calculate the time of emergence at each point on the globe assuming a 1.0 ppb/decade trend everywhere. We choose 1.0 ppb/decade as this is the order of magnitude of the forced trends under the RCP scenarios (see Figures 9a and 10a). While it is certainly unphysical to expect an identical forced trend in surface ozone at all locations, this exercise identifies the regions and seasons where the time of emergence is most sensitive to internal climate variability.

Figure 8 shows the year of emergence of a 1.0 ppb/decade forced trend assuming a start year of 2006. Later, emergence years are denoted by warm colors and highlight regions where large internal variability delays the emergence of the forced signal from internal climate variability until 2025 or later. Western Europe exhibits long emergence times of a 1 ppb/decade trend in winter (2045 or later); thus, it may be very difficult in these regions to detect forced trends in surface ozone on short time scales. On the other hand, the small values in Figure 8 highlight the regions and seasons that are least sensitive to meteorologically driven trends, and thus, locations where a forced trend may be more easily detected. For example, a 1 ppb/decade trend in winter over China would emerge by 2025, indicating that 20 year record lengths would be sufficient to detect a trend of this magnitude there. We emphasize, however, that smaller forced trends in this region would take longer to detect. Finally, note that as expected, the regions with the longest emergence times correspond to the regions with the largest spreads in 20 year trends (Figure 6). If seasonal surface ozone were perfectly Gaussian and if we had an infinite amount of data, Figures 8 and 6 would be exact rescalings of one another due to the relationship between the time of emergence (as defined here) and the standard deviation of the internal variability (see section 2.3).

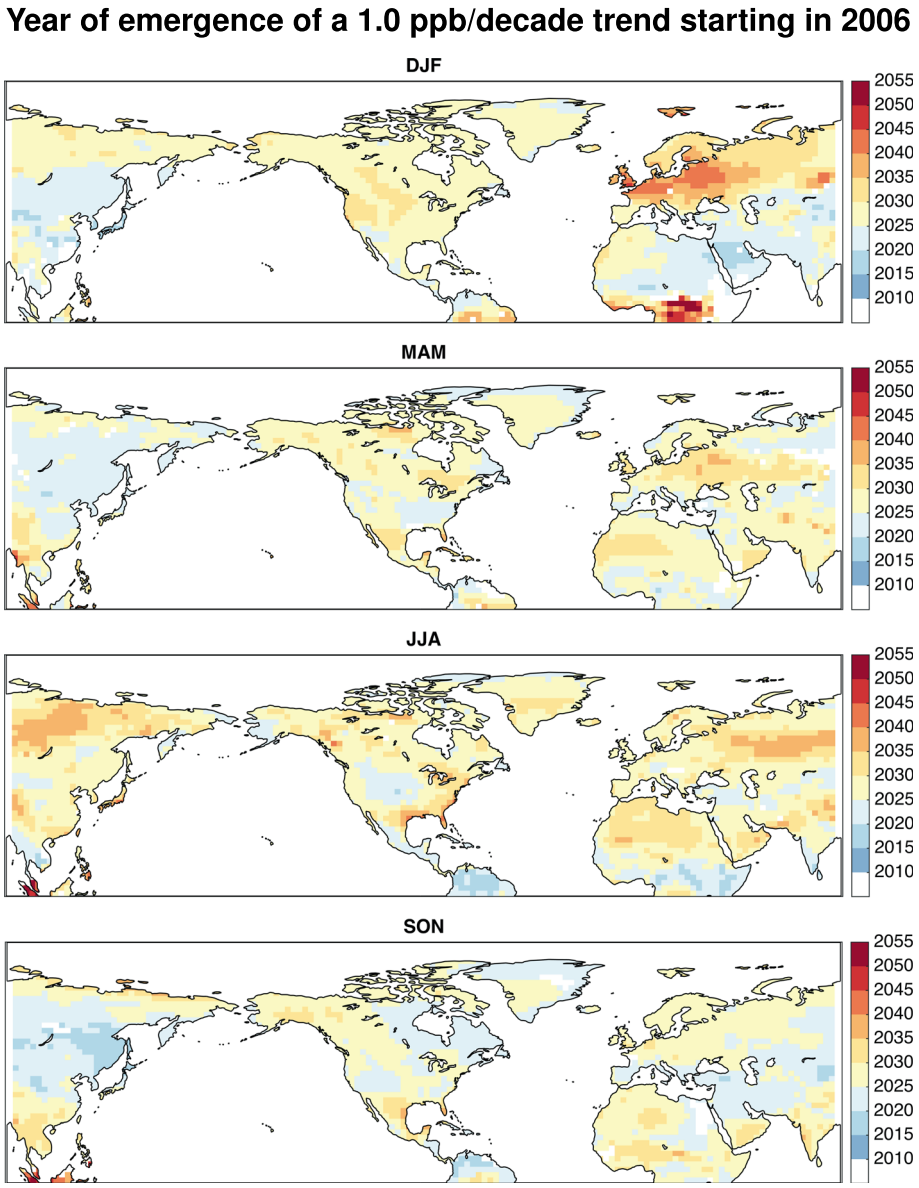

Figure 8. The year of emergence of a 1.0 ppb/decade surface ozone trend starting in 2006.

While Figure 8 displays regions where internal climate variability will matter most for detecting a homogeneous surface ozone trend, it is expected that surface ozone trends in the future will vary by location and scenario due to different regional emission trends and regional responses to climate forcing. Thus, we plot in Figure 9 the full time of emergence when both the internal variability and forced response, as represented by the RCP4.5 scenario, are considered. Figure 9a depicts the forced trend, estimated as the mean trend in surface ozone in RCP4.5 between 2006 and 2055 across all three ensemble members. Figure 9b provides an estimate of the year when the forced signal will emerge, that is, when one can be confident that the data will exhibit a trend of the same sign as the forced trend.

The forced trend in surface ozone under RCP4.5 (that is, the trend attributable to the combined effects of changing ozone precursor emissions and increasing greenhouse gas concentrations) is positive over the continents during winter and negative during summer (Figure 9a). This seasonality mainly reflects NO_x reductions which act to lower surface ozone in summer but slightly increase it in winter due to reduced titration [*Clifton et al.*, 2014; *Simon et al.*, 2015; *Gao et al.*, 2013]. The time of emergence (Figure 9b) is shortest for regions with large forced trends and small internal variability (e.g., winter over the northeast United States) and longest for

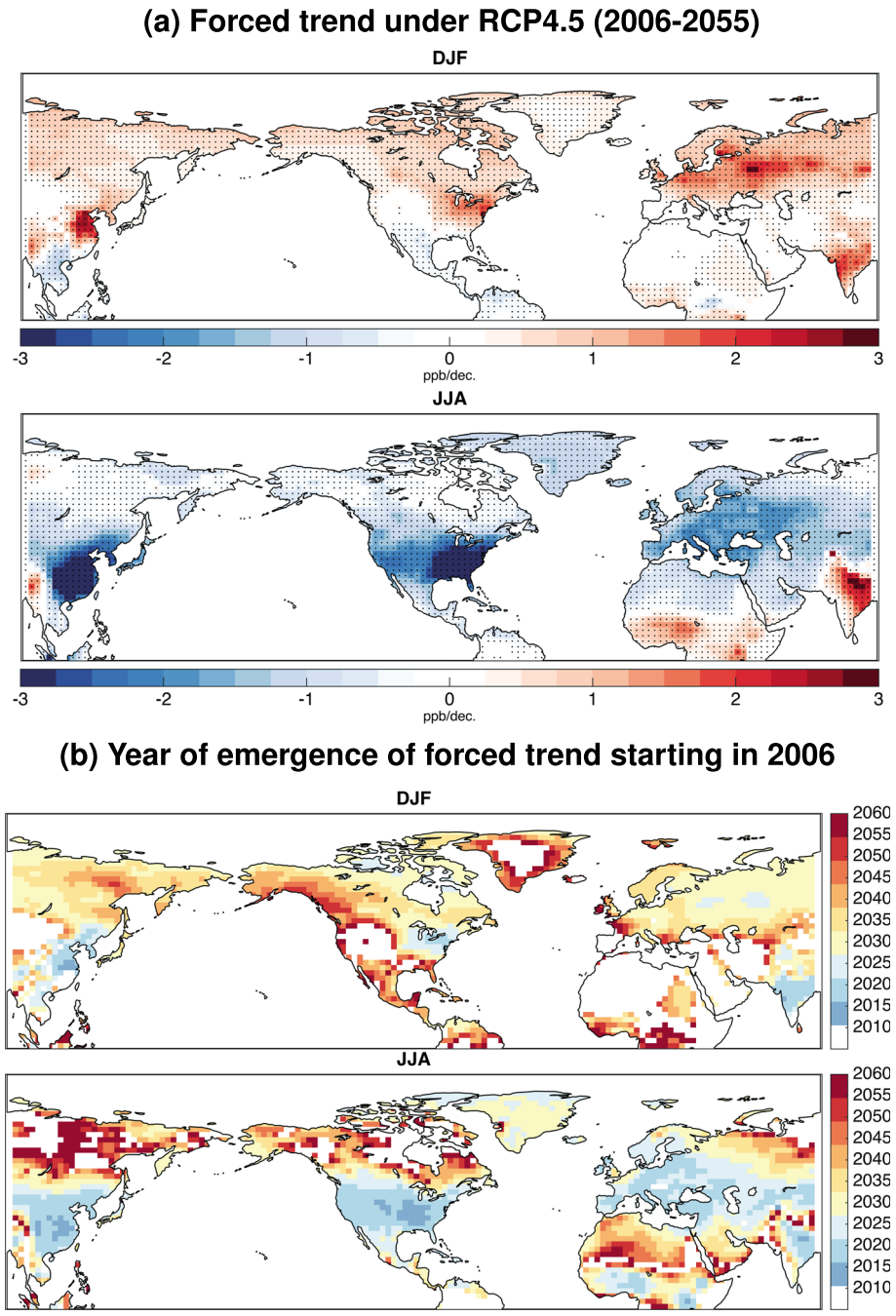

Figure 9. (a) The ensemble mean 2006–2055 trend in surface ozone in the full RCP4.5 simulations. (b) The year of emergence of the forced trend in RCP4.5. Stippling in Figure 9a denotes trends that are significant at the 95% level, and regions where the ensemble mean trend magnitude is less than 0.25 ppb/dec are masked out.

regions with small forced trends and large internal variability (e.g., eastern Russia). Note that western Europe and eastern North America have similar forced trends in winter (Figure 9a); however, their emergence times differ by at least 10 years (Figure 9b) due to the larger internal climate variability over western Europe in this season (refer to Figures 6 and 8).

Figure 10 shows similar panels for RCP8.5. Under this scenario, the forced surface ozone trend (Figure 10a) is larger over the entire Northern Hemisphere than in RCP4.5, reflecting the large increase in global methane and ensuing rise in background tropospheric ozone. In summer, the forced trend over North America is

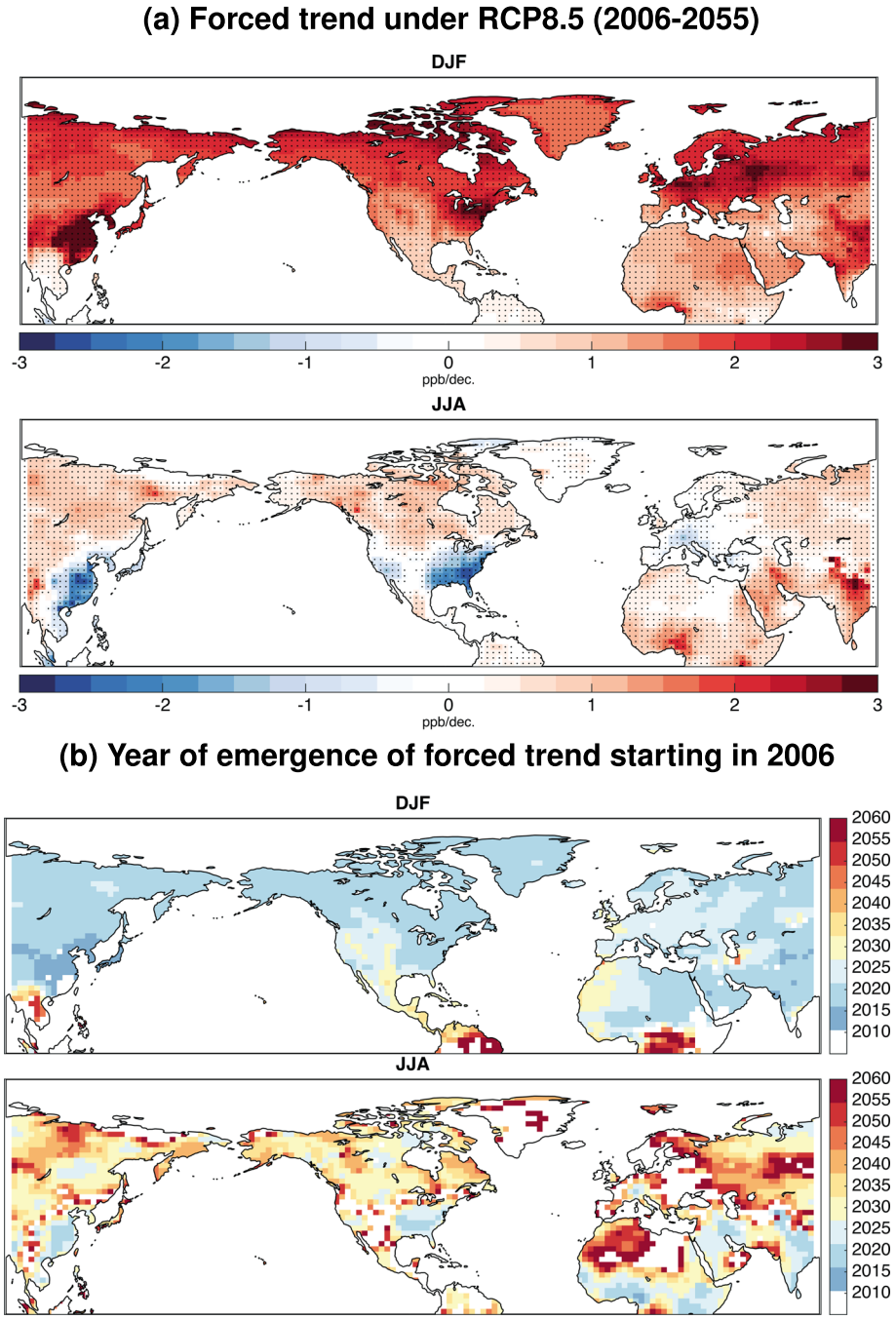

Figure 10. (a) The ensemble mean 2006–2055 trend in surface ozone in the full RCP8.5 simulations. (b) The year of emergence of the forced trend in RCP8.5. Stippling in Figure 10a denotes trends that are significant at the 95% level, and regions where the ensemble mean trend magnitude is less than 0.25 ppb/dec are masked out.

negative due to reduced NO_x emissions but positive over Asia. As was the case for RCP4.5, emergence times vary spatially due to regional differences in forced trends and climate variability. The largest difference between RCP8.5 and RCP4.5 is that the forced trends over most of North America in DJF are projected to emerge by 2035 under RCP4.5 but 2015 under RCP8.5 due to the larger forced trends for this scenario. The unforced climate variability of surface ozone in all model simulations is assumed to equal that in the Control-1990 simulation (Figure 4, see section 2.3 for details), and so differences in the time of emergence between scenarios can be attributed to differences in the forced trend.

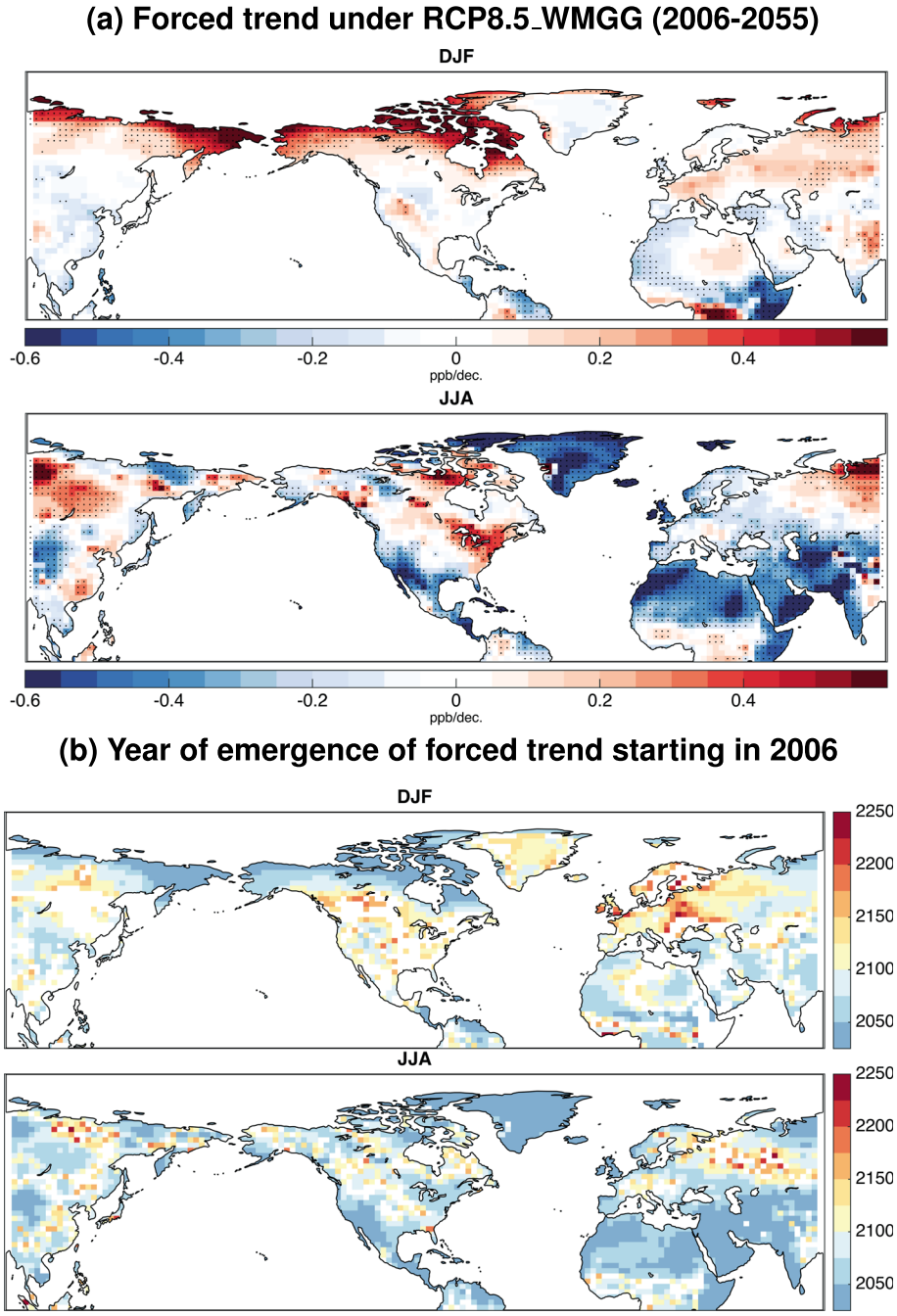

Figure 11. (a) The ensemble mean 2006–2055 trend in surface ozone in the RCP8.5_WMGG simulations. (b) The year of emergence of the forced trend in RCP8.5_WMGG. Stippling in Figure11a denotes trends that are significant at the 95% level, and regions where the ensemble mean trend magnitude is less than 0.05 ppb/dec are masked out.

The time of emergence of a surface ozone trend in RCP8.5 includes components forced by ozone and aerosol precursor emissions and greenhouse gas increases. RCP8.5_WMGG, on the other hand, includes only greenhouse gas increases since ozone and aerosol precursor emissions are held fixed. Using this scenario, we can estimate the trends in surface ozone driven solely by increasing greenhouse gases in the absence of ozone precursor emissions and quantify the time it would take for such a signal to emerge from the noise. Figure 11 shows results for RCP8.5_WMGG analogous to Figure 10, although the scales are different between the two figures. Greenhouse gas increases are projected to increase wintertime surface ozone at high latitudes and

decrease summertime surface ozone over much of the subtropics (trends are similar but slightly weaker for RCP4.5_WMGG). Summertime increases are found, however, over eastern North America and northern Russia, most likely because greenhouse gas emissions are leading to conditions that increase surface ozone in already polluted regions (e.g., warmer temperatures and more stagnation) [e.g., *Fiore et al.*, 2015]. Focusing on the annual mean surface ozone response to climate change in the absence of precursor emission changes, *Doherty et al.* [2013] found similar increases over North America in three different atmosphere-only chemistry climate models and a general decrease in annual mean surface ozone over Africa and Greenland, as found here in JJA.

The surface ozone trends simulated in RCP8.5_WMGG (Figure 11a) tend to be 2 to 3 times smaller than those in the full RCP8.5 simulation (Figure 10a), highlighting the dominant role of ozone precursor emissions in driving future forced trends which may amplify or offset any forced trend due to anthropogenic climate change. Due to the smaller forced trends when emissions are held fixed, the time of emergence of the forced trends under RCP8.5_WMGG can be very long. For example, trends over eastern Europe would not emerge until 2200, if the trend remained linear far into the future. Even the forced trends with the earliest year of emergence do not emerge until after 2025. These simulations thus suggest that while most precursor emissions-driven trends in surface ozone would emerge before 2055, trends due to increasing greenhouse gas emissions alone would emerge much later.

5. Conclusions

Using over 1000 years of model simulations of the GFDL CM3 coupled chemistry-climate model, we explore the role of internal climate variability in driving multi-decadal trends in surface ozone. We then discuss how these trends may be superimposed on future forced trends driven by emissions changes and anthropogenic climate change. While the results from this analysis are shown to be sensitive to the particular future scenario analyzed (e.g., RCP4.5 or RCP8.5), we can summarize our general findings in five main conclusions:

1. Internal climate variability alone can drive multidecadal trends as large as those driven by changes in emissions.
2. A uniform global forced trend in surface ozone is most difficult to detect in regions and seasons with large internal surface ozone variability (e.g., western Europe in winter) and easiest to detect in regions with small internal surface ozone variability (e.g., eastern Asia in autumn). Thus, knowledge of the level of regional climate-induced ozone variability may be used to guide deployment of measurement sites intended to track long-term trends in atmospheric composition (e.g., Global Atmospheric Watch sites).
3. The magnitude of unforced variability and forced trends can exhibit large seasonality, and thus, a given trend in regional surface ozone may emerge earlier in some seasons (i.e., autumn) than in others (i.e., winter). Specifically, for a uniform, global forced trend, the regions where we would expect to first be able to detect the trend with confidence are the northeast U.S. in spring, the U.S. mountain west in summer, western Europe in autumn, and eastern Asia in winter and autumn.
4. The time of emergence of a forced trend in surface ozone is determined by both (1) the magnitude of the forced trend and (2) the local unforced variability. Both of these factors contribute substantially to dictating the geographic heterogeneity in the time of emergence.
5. Simulated surface ozone trends over the first half of the 21st century are driven predominantly by changes in ozone precursor emissions and internal climate variability, with trends due to increasing greenhouse gas emissions alone playing a minor role under the RCP4.5 and RCP8.5 scenarios.

Our results highlight the influential role of climate variability in driving a wide range of surface ozone trends. It follows that direct comparisons of modeled and observed trends in surface ozone will remain a challenge, since differences between modeled and observed trends may reflect climate noise rather than model deficiencies.

The results highlighted here were determined from the simulations with one chemistry-climate model (CM3), and thus, similar analysis should be performed for other climate models to determine the robustness of the regional and seasonal conclusions described here. Chemistry-climate model intercomparisons, such as CCMI, will be a good place to start. However, we expect our main conclusion to hold; namely, that climate variability is capable of driving large multidecadal trends in surface ozone. Finally, while our focus here has been on global surface ozone, the role of internal climate variability in driving multidecadal trends should apply more generally to any reactive trace atmospheric constituent.

Acknowledgments
We are grateful to Gus Correa for assisting with processing and archival of model simulations. The observational ozone record from Zugspitze, Germany, was provided by Hans-Eckhart Scheel. E.A.B. is supported, in part, by NSF grant AGS-1419818. A.M.F. acknowledges support from EPA STAR grant 83520601. This article's contents are solely the responsibility of the grantee and do not necessarily represent the official view of the EPA. Further, the EPA does not endorse the purchase of any commercial products or services mentioned in the publication. The data used are listed in the references and table and are available upon request. The authors also thank three anonymous reviewers for their helpful comments on an earlier version of this manuscript.

References

Austin, J., L. W. Horowitz, M. D. Schwarzkopf, R. J. Wilson, and H. Levy (2013), Stratospheric ozone and temperature simulated from the preindustrial era to the present day, *J. Clim.*, *26*, 3528–3543, doi:10.1175/JCLI-D-12-00162.1.

Barnes, E. A., and A. M. Fiore (2013), Surface ozone variability and the jet position: Implications for projecting future air quality, *Geophys. Res. Lett.*, *40*, 2839–2844, doi:10.1002/grl.50411.

Clifton, O. E., A. M. Fiore, G. Correa, L. W. Horowitz, and V. Naik (2014), Twenty-first century reversal of the surface ozone seasonal cycle over the northeastern United States, *Geophys. Res. Lett.*, *41*, 7343–7350, doi:10.2002/2014GL061378.

Cooper, O. R., et al. (2010), Increasing springtime ozone mixing ratios in the free troposphere over western North America, *Nature*, *463*(7279), 344–348, doi:10.1038/nature08708.

Doherty, R. M., et al. (2013), Impacts of climate change on surface ozone and intercontinental ozone pollution: A multi-model study, *J. Geophys. Res. Atmos.*, *118*, 3744–3763, doi:10.1002/jgrd.50266.

Donner, L. J., et al. (2011), The dynamical core, physical parameterizations, and basic simulation characteristics of the atmospheric component AM3 of the GFDL Global Coupled Model CM3, *J. Clim.*, *24*, 3484–3519, doi:10.1175/2011JCLI3955.1.

Eyring, A., et al. (2013), Overview of IGAC/SPARC Chemistry-Climate Model Initiative (CCMI) community simulations in support of upcoming ozone and climate assessments, *SPARC Newsletter*, *40*, 48–66.

Fiore, A., et al. (2014), Estimating North American background ozone in U.S. surface air with two independent global models: Variability, uncertainties, and recommendations, *Atmos. Environ.*, *96*, 284–300, doi:10.1016/j.atmosenv.2014.07.045.

Fiore, A. M., V. Naik, and E. M. Leibensperger (2015), Air quality and climate connections, *J. Air Waste Manage. Assoc.*, *65*, 645–685, doi:10.1080/10962247.2015.1040526.

Gao, Y., J. S. Fu, J. B. Drake, J. F. Lamarque, and Y. Liu (2013), The impact of emission and climate change on ozone in the United States under representative concentration pathways (RCPs), *Atmos. Chem. Phys.*, *13*, 9607–9621, doi:10.5194/acp-13-9607-2013.

Hess, P., D. Kinnison, and Q. Tang (2015), Ensemble simulations of the role of the stratosphere in the attribution of northern extratropical tropospheric ozone variability, *Atmos. Chem. Phys.*, *15*(5), 2341–2365, doi:10.5194/acp-15-2341-2015.

John, J. G., A. M. Fiore, V. Naik, L. W. Horowitz, and J. P. Dunne (2012), Climate versus emission drivers of methane lifetime from 1860–2100, *Atmos. Chem. Phys.*, *12*, 12,021–12,036, doi:10.5194/acp-12-12021-2012.

Lamarque, J. F., D. T. Shindell, and E. A. B. Josse (2013), The Atmospheric Chemistry and Climate Model Intercomparison Project (ACCMIP): Overview and description of models, simulations and climate diagnostics, *Geosci. Model Dev.*, *6*, 179–206, doi:10.5194/gmd-6-179-2013.

Lamarque, J. F., et al. (2012), CAM-chem: Description and evaluation of interactive atmospheric chemistry in the Community Earth System Model, *Geosci. Model Dev.*, *5*, 369–411, doi:10.5194/gmd-5-369-2012.

Levy, H., L. W. Horowitz, M. D. Schwarzkopf, Y. Ming, J.-C. Golaz, V. Naik, and V. Ramaswamy (2013), The roles of aerosol direct and indirect effects in past and future climate change, *J. Geophys. Res. Atmos.*, *118*, 4521–4532, doi:10.1002/jgrd.50192.

Lin, M., A. M. Fiore, O. R. Cooper, L. W. Horowitz, A. O. Langford, H. Levy II, B. J. Johnson, V. Naik, S. J. Oltmans, and C. J. Senff (2012), Springtime high surface ozone events over the western United States: Quantifying the role of stratospheric intrusions, *J. Geophys. Res. Atmos.*, *117*, D00V22, doi:10.1029/2012JD018151.

Lin, M., L. W. Horowitz, S. Oltmans, A. M. Fiore, and S. Fan (2014), Tropospheric ozone trends at Mauna Loa Observatory tied to decadal climate variability, *Nat. Geosci.*, *7*, doi:10.1038/ngeo2066.

Lin, M., A. M. Fiore, L. W. Horowitz, A. O. Langford, S. J. Oltmans, D. Tarasick, and H. E. Rieder (2015a), Climate variability modulates western US ozone air quality in spring via deep stratospheric intrusions, *Nat. Commun.*, *6*, 7105, doi:10.1038/ncomms8105.

Lin, M., L. W. Horowitz, O. R. Cooper, D. Tarasick, S. Conley, L. T. Iraci, B. Johnson, T. Leblanc, I. Petropavlovskikh, and E. L. Yates (2015b), Revisiting the evidence of increasing springtime ozone mixing ratios in the free troposphere over western North America, *Geophys. Res. Lett.*, *42*, 8719–8728, doi:10.1002/2015GL065311.

McClure-Begley, A., I. Petropavlovskikh, and S. Oltmans (2014), NOAA global monitoring surface ozone network, in *National Oceanic and Atmospheric Administration, Earth Systems Research Laboratory Global Monitoring Division*, Boulder, Colo., doi:10.7289/V57P8WBF.

Naik, V., L. W. Horowitz, A. M. Fiore, P. Ginoux, J. Mao, A. M. Aghedo, and H. Levy (2013), Impact of preindustrial to present-day changes in short-lived pollutant emissions on atmospheric composition and climate forcing, *J. Geophys. Res. Atmos.*, *118*, 8086–8110, doi:10.1002/jgrd.50608.

Parrish, D., et al. (2012), Long-term changes in lower tropospheric baseline ozone concentrations at northern mid-latitudes, *Atmos. Chem. Phys.*, *12*, 11,485–11,504, doi:10.5194/acp-12-11485-2012.

Parrish, D., et al. (2014), Long-term changes in lower tropospheric baseline ozone concentrations: Comparing chemistry-climate models and observations at northern midlatitudes, *J. Geophys. Res. Atmos.*, *119*, 5719–5736, doi:10.1002/ 2013JD021435.

Simon, H., A. Reff, B. Wells, J. Xing, and N. Frank (2015), Ozone trends across the United States over a period of decreasing NOx and VOC emissions, *Environ. Sci. Technol.*, *49*(1), 186–195, doi:10.1021/es504514z.

Thompson, D. W. J., E. Barnes, C. Deser, W. Foust, and A. Phillips (2015), Quantifying the role of internal climate variability in future climate trends, *J. Clim.*, *28*, 6443–6456, doi:10.1175/JCLI-D-14-00830.1.

Turner, A. J., A. M. Fiore, L. W. Horrowitz, V. Naik, and M. Bauer (2013), Summertime cyclones over the Great Lakes Storm Track from 1860–2100: Variability, trends and association with ozone pollution, *Atmos. Chem. Phys.*, *13*, 565–578, doi:10.5194/acp-13-565-2013.

Wild, O., et al. (2012), Modelling future changes in surface ozone: A parameterized approach, *Atmos. Chem. Phys.*, *12*, 2037–2054, doi:10.5194/acp-12-2037-2012.